LANGMUIR

pubs.acs.org/Langmuir Article

Unraveling the Nano–Bio Interface Interactions of a Lipase Adsorbed on Gold Nanoparticles under Laser Excitation

Heloise Ribeiro de Barros,* Rafael Trivella Pacheco da Silva, Rafaella Fernandes, Jhoan Toro-Mendoza, Ivan Coluzza, Marcia L. A. Temperini, and Susana I. Cordoba de Torresi*

Cite This: *Langmuir* 2024, 40, 5663–5672 Read Online

ACCESS | Metrics & More | Article Recommendations | Supporting Information

ABSTRACT: The complex nature and structure of biomolecules and nanoparticles and their interactions make it challenging to achieve a deeper understanding of the dynamics at the nano–bio interface of enzymes and plasmonic nanoparticles subjected to light excitation. In this study, circular dichroism (CD) and Raman spectroscopic experiments and molecular dynamics (MD) simulations were used to investigate the potential changes at the nano–bio interface upon plasmonic excitation. Our data showed that photothermal and thermal heating induced distinct changes in the secondary structure of a model nanobioconjugate composed of lipase from *Candida antarctica* fraction B (CALB) and gold nanoparticles (AuNPs). The use of a green laser led to a substantial decrease in the α-helix content of the lipase from 66% to 13% and an increase in the β-sheet content from 5% to 31% compared to the initial conformation of the nanobioconjugate. In contrast, the differences under similar thermal heating conditions were only 55% and 11%, respectively. This study revealed important differences related to the enzyme secondary structure, enzyme–nanoparticle interactions, and the stability of the enzyme catalytic triad (Ser105-Asp187-His224), influenced by the instantaneous local temperature increase generated from photothermal heating compared to the slower rate of thermal heating of the bulk. These results provide valuable insights into the interactions between biomolecules and plasmonic nanoparticles induced by photothermal heating, advancing plasmonic biocatalysis and related fields.

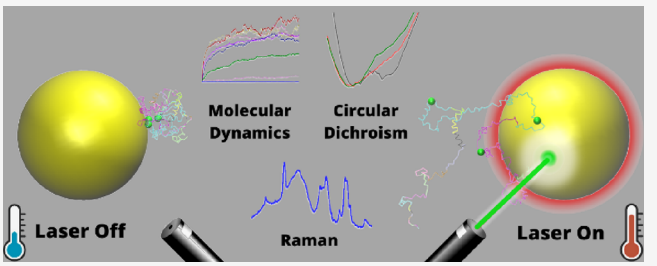

INTRODUCTION

Understanding the biophysicochemical interactions at the nano–bio interface between nanoparticles (NPs) and biomolecules is a challenging task due to the complex nature of these interactions,[1−4] as they are dependent on external factors such as adsorption orientation and medium conditions (temperature, pH, ionic strength, etc.).[5−8] Notably, these interactions might impact the functionality and, as a consequence, biocatalytic response of enzymes in specific reactions.[9,10] In that way, understanding the potential changes in biophysicochemical interactions upon light excitation is of foremost importance for predicting the effects of light on enzyme functionality for applications in light-driven reactions and ensuring the performance of engineered nanobioconjugates. In particular, the effects generated from the localized surface plasmon resonance (LSPR) excitation of plasmonic NPs can lead to enhanced performance of biocatalysts coupled to their surface, which has gained significant relevance as a novel strategy to improve biocatalysis.[5,10] This emerging field of study, recently named plasmonic biocatalysis, explores the improvement of biocatalytic performance by remote regulation of enzyme properties via noninvasive strategies.[11] Previous studies have shown the effect of laser stimuli on biocatalytic activity using different enzymes and supports.[11−16] However, although these studies analyzed the interactions between enzymes and metallic nanoparticles, the changes in their secondary structure and enzyme–nanoparticle interactions induced by laser irradiation have largely been underexplored. However, the impacts of LSPR excitation at the nano–bio interface need to be further studied. This approach is fundamental for understanding the transformations in light-driven reactions at the nanoscale level and providing important information for the rational design of different LSPR-driven biocatalytic systems. Furthermore, this information is important for determining the colloidal stability of these nanobioconjugates upon laser irradiation to ensure the desired properties of plasmonic NPs and their optical applications.[17]

In this work, our goal was to elucidate different aspects of the enzyme conformation at the nano–bio interface of a nanobioconjugate upon laser irradiation. Among the main LSPR outcomes, such as the formation of hot carriers, near-

Received: October 5, 2023
Revised: February 21, 2024
Accepted: February 23, 2024
Published: March 7, 2024

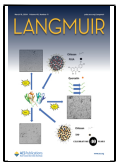

https://doi.org/10.1021/acs.langmuir.3c02994
Langmuir 2024, 40, 5663–5672

field enhancement, and heat generation,[18] the scope of this work is to study the photothermal influence on a nonredox enzymatic system. We performed a detailed study using Raman and circular dichroism (CD) spectroscopic experiments to assess nanoparticle-enzyme interactions at the molecular level. A comparison of the chemical changes resulting from nonirradiated conditions and bulk temperature changes resulting from thermal and photothermal heating was demonstrated and explained. Molecular dynamics (MD) simulations were carried out to correlate the findings for the enzyme unfolding obtained by spectroscopic techniques and the stability of the catalytic triad with an increasing temperature. To accomplish this goal, we analyzed a role model system composed of lipase from *Candida antarctica* fraction B (CALB) adsorbed on spherical gold nanoparticles (AuNPs) as a proof-of-concept system. The nanobioconjugate was excited by a green laser source (λ = 532 nm), which is in resonance with the excitation wavelength of the AuNPs, with an LSPR band maximum of approximately 520 nm. A near-infrared (NIR) (λ = 808 nm) laser source was also applied in some cases to achieve out-of-resonance conditions. Although the mechanisms underlying the influence of lasers on the biocatalysis of these nanobioconjugates were previously elucidated using AuNPs with different morphologies,[11] a clear understanding of the interactions between the enzymes and their interactions with plasmonic NPs under laser irradiation has not been achieved.[19] Thus, herein, we present significant findings indicating unique conformational changes in CALB when it interacts with the AuNP surface promoted by photothermal heating rather than thermal heating.

EXPERIMENTAL SECTION

Materials. Sodium citrate tribasic dehydrate, tetrachloroauric(III) acid ($HAuCl_4$), phosphate-buffered saline (PBS) (pH 7.4), and lipase from *Candida antarctica* fraction B (CALB) were purchased from Sigma-Aldrich. The CALB concentration was determined by the Bradford colorimetric method.[20] All chemicals were used as received. Purified Milli-Q water (Millipore, 18.2 MΩ cm) was used in the preparation of all of the solutions.

AuNP Synthesis. AuNPs were prepared through the typical Turkevich method,[21] in which, for 30 mL of H_2O, 900 μL of a 1% (w/w) solution of sodium citrate in water was heated to boiling on a heating plate with magnetic stirring, followed by the addition of 300 μL of 25 mmol L^{-1} $HAuCl_4$. The mixture was stirred for 15 min and allowed to cool to room temperature before being stored in a refrigerator for subsequent use.

CALB@AuNP Synthesis. The adsorption of CALB on the AuNPs was performed according to a previously described method.[11] Briefly, 10 mL of the previously synthesized AuNPs and 10 mL of CALB solution in PBS at pH 7.4 (0.1 mg mL^{-1}) were added to a round-bottom flask placed at 32 °C for 2 h in a bath on a heat plate. Subsequently, the mixture was preserved at 4 °C until use. For analysis, this sample was washed to remove the unadsorbed CALB and unreacted CALB from the synthesized AuNPs by centrifugation at 13,000 rpm for 20 min. The supernatant was removed, and the pellet was redispersed in PBS. This procedure was performed once since after two rounds of redispersion and centrifugation, we clearly observed that no CALB was desorbed from the AuNPs by analyzing the supernatant according to the characteristic protein absorbance peak at λ = 280 nm in the UV−vis spectrum. The final molar concentration of Au was 0.5 μmol L^{-1}, as determined by UV−vis spectroscopy using the typical signal (λ = 400 nm) corresponding to the Au concentration.[22] The final concentration of CALB in the bioconjugate CALB@AuNP was 0.8 μmol L^{-1}.

TEM Characterization. CALB@AuNPs were characterized via TEM using a JEOL JEM-1400 PLUS microscope at an acceleration voltage of 120 kV. Samples were prepared by drop casting 3 μL of the sample on lacey carbon-coated copper grids and left to dry.

Laser Apparatus. Experiments involving laser irradiation were performed by using two different laser sources. The NIR laser used was at λ = 808 nm (fiber-coupled laser diode, Lumics LU0808T040), and the green laser was at λ = 532 nm (fiber-coupled laser diode, CNI MGL-FN-532) with adjustable power densities. Both laser sources illuminated the samples through two lenses, one to collimate and the other to expand the laser beam adjusted to illuminate a spot of 1 cm^2 of the sample in a cuvette. The power density used in the experiments was 1.4 W/cm^2.

Thermal Camera Analysis. Thermal camera analyses were performed by placing the equipment (FLIRA35) 15 cm above the cuvette. The heating and cooling curves were obtained using ResearchIR software after discounting the blank curves generated with PBS.

CD Spectroscopy. CD spectroscopy was performed with a Jasco J-815 spectrometer, ranging from 190 to 260 nm with a scanning speed of 50 nm min^{-1}, a bandwidth of 1 nm, and a data pitch of 0.5 nm. A quartz cuvette with a path length of 1 mm was used, and the temperature was controlled by a Peltier system whenever the temperature ramps were applied. The spectra were recorded as an average of 10 accumulations, and the CD spectra were corrected against the water blank. Secondary structures were obtained from CD data analyzed using Dichroweb with the K2D model.[23]

Raman Spectroscopy. Raman spectra were acquired using a Renishaw inVia Reflex fitted with a Peltier cooled CCD camera (Renishaw, 600 × 400 pixels) coupled to a Leica Microscope (DM2500M). The spectra were obtained using a 785 nm laser line focused on the samples by a 20× Leica objective (NA 0.40). All Raman spectra were acquired through 2 scans with a 20 s accumulation time.

Molecular Dynamics Calculations. We performed coarse-grained molecular dynamics simulations of CALB in the presence of charged spherical NPs using the LAMMPS package.[24,25] Because we aimed to characterize the protein structural changes induced by the adsorption of the NPs, we focused the protein modeling on a computationally efficient description of the native state. For that purpose, we represented the CALB using a GO-type protein model developed by Baumketner et al.[26] The folded state is imposed as the global free-energy minimum in these model types. The rationale behind such an approach is that the folding landscape follows the minimum-frustration principle introduced by Wolynes and Onuchic.[27] Hence, the configurational space close to the native state is accurately modeled. All attractive interactions (residue−residue, oppositely charged residue−polymer, and HB interactions) are represented with a sigmoidal-type potential UATT used in coarse-grained protein models to represent residue−residue interactions.

As stated in a previous paper, all attractive interactions (residue−residue and oppositely charged residue-NP interactions) are represented by a sigmoidal-type potential UATT used in coarse-grained protein models to represent residue−residue interactions.

$$U_{\mathrm{ATT}} = \frac{1}{1.0 + e^{-2.5(r_c - r)}}$$

The solvent is implicit. On the other hand, all excluded volume interactions are represented by a Weeks−Chandler−Andersen potential, which is a Lennard-Jones potential that is shifted to zero from the distance corresponding to the minimum to infinity. Although the representation of the electrostatic interaction is not physically accurate, it still captures the short-range attractions that hold the protein on to the surfaces of the NPs and cause protein conformational changes, all at a fraction of the computational cost. Moreover, we did not observe any point in the coupling of GO potentials to accurate electrostatic interactions. Our approach left us with a free parameter, namely, the relative ratio between the residue−residue and the residue-NP interactions.

Additionally, in a previous report, a numerical protocol was developed in which the interactions between the different residues and the surface charges of the NPs were included.[28] Hence, we

https://doi.org/10.1021/acs.langmuir.3c02994
Langmuir 2024, 40, 5663−5672

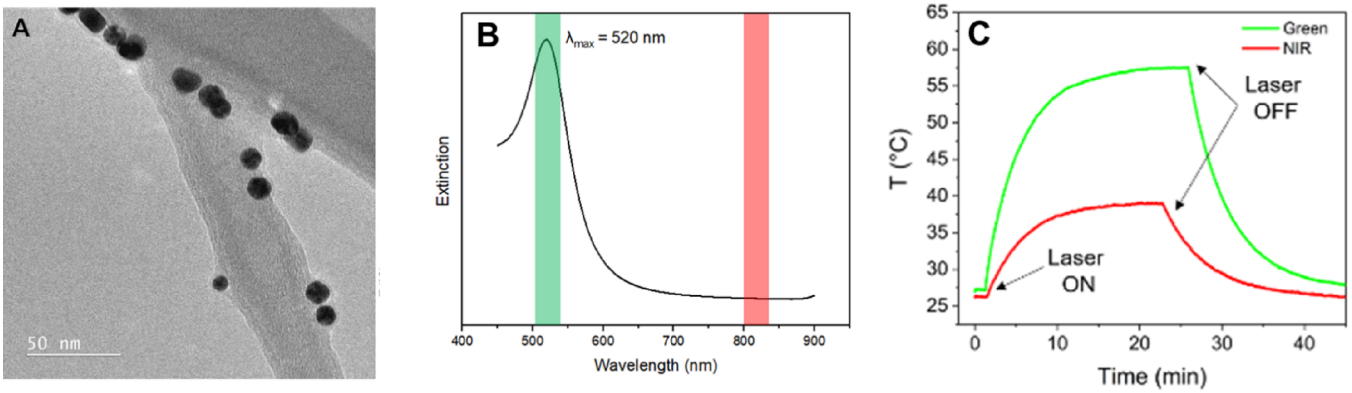

Figure 1. (A) TEM image of the as-prepared CALB@AuNPs. (B) Extinction spectrum and LSPR band of CALB@AuNPs, where green and red bars indicate the wavelength range from the laser sources applied (λ = 532 and 808 nm). (C) Representative temperature monitored by a thermal camera of a cuvette containing the colloidal dispersion of CALB@AuNPs during irradiation by green and NIR laser at a power density of 1.4 W/cm^2 for at least 20 min.

developed a coarse-grained representation of the protein-NP system based on the one used in our previous study.[29] The acceptor and donor states are determined from the ζ-potential using the expression from Ohshima et al.

$$\sigma_\zeta = \frac{2\varepsilon_r\varepsilon_0\kappa kT}{e}\sin h\sin h\left(\frac{e\zeta}{2kT}\right)\left[1 + \frac{1}{\kappa a}\left(\frac{2}{\cos h^2\left(\frac{e\zeta}{4kT}\right)}\right) + \frac{1}{(\kappa a)^2}\left(\frac{8\ln\left[\cos h\cos h\left(\frac{e\zeta}{4kT}\right)\right]}{\sin h^2\left(\frac{e\zeta}{2kT}\right)}\right)\right]^{1/2}$$

where ε_r = 80.2 is the relative permittivity of water at room temperature, 8.85 × 10ε_0^{-12} C/Nm^2 is the permittivity of vacuum, κ^{-1} is the Debye length estimated at 0.7 nm under physiological conditions, e = 1.6 × 10^{-19} C is the elementary electric charge, kT = 4.11 × 10^{-19} J is the thermal energy, and the ζ potential is estimated in the experiments. Here, we determined the protonation state of CALB using the PropKA software package.

Molecular dynamics calculations were performed by using the LAMMPS package. From the PDB file obtained from the Protein Database (code 1TCA), the first calculation of structural stability was performed. Then, an additional "atom" was added to both the input and coordinate files to model the presence of the nanoparticle. The interactions between the different residues and the NP consisted of sigmoidal interactions, including repulsive and attractive forces, depending on the electric charge of each surface residue and that of the NP. The magnitude of the force interaction was studied by using 60 LJ potential strength units. All of the calculations were performed at constant temperature and pressure, implicit solvent, using a Langevin thermostat for 1 M steps in a single run under an NVE integration scheme. The results were analyzed in terms of the mean square displacement of CALB and the radial distribution function of the indicated residues. The values of the parameters in the LJ units are temperature (T*), mass, epsilon = 1, time step = 0.002, and sigma = 4. The particles were placed in the center of a cubic box large enough to avoid periodic boundary condition effects.

RESULTS AND DISCUSSION

The AuNPs were obtained via Turkevich et al.'s method.[21] The particles obtained were spherical and monodispersed in size with an average diameter of 13 ± 2 nm, as observed by transmission electron microscopy (TEM) images and their LSPR in the UV−vis spectrum (Figure S1). CALB was immobilized onto the NP surface via physisorption to allow close contact between the parts, as previously described.[30] The obtained nanobioconjugate was referred to as CALB@AuNP. It is well established that the surface of AuNPs is highly favorable for protein adsorption, mainly through electrostatic interactions or covalent bonding via thiol groups.[30,31] The amino groups present in the CALB structure are also favorable for interacting with the carboxyl groups on the surface of the AuNPs that remain from citrate-driven reduction and stabilization. Additionally, the structure of CALB contains 6 cysteine and 4 methionine residues,[32] which possess thiolated groups that thermodynamically preferentially interact with the AuNP surface.[33,34] Ultimately, CALB and AuNPs are expected to interact through subsequent anchoring, crawling, and binding kinetic processes.[31,35]

The morphology and size of the synthesized AuNPs were maintained after CALB adsorption (Figure 1A). In addition, no particle aggregation was observed, which confirmed the preservation of the colloidal stability and characteristics of the AuNPs after the formation of the nanobioconjugate. Moreover, further colloidal stability and protein corona formation analyses of CALB@AuNPs were performed in a previous study by our group.[30] We herein applied and compared green and NIR (λ = 532 and 808 nm, respectively) laser irradiation of the CALB@AuNP colloidal suspension. Figure 1B shows the LSPR band of AuNPs in the extinction spectra alongside the representation of the wavelength range of the green (green bar) and NIR (red bar) laser sources employed in the study. By using a thermal camera positioned close to the reaction vessel, we were able to monitor the temperature increase throughout the media resulting from laser irradiation. Both laser sources were applied at the same power density (1.4 W/cm^2) for 20 min to the colloidal suspension of CALB@AuNPs at the same concentration in a quartz cuvette. Interestingly, we clearly observed a temperature increase in the colloidal media when the media were illuminated by both lasers, followed by exponential decay when the lasers were turned off (Figure 1C). On the one hand, upon irradiation with the NIR laser source, which is out of resonance with the LSPR of CALB@AuNPs, and a temperature increase (ΔT) of only 13 °C was observed. On the other hand, upon irradiation with the green laser source, which is in resonance with the LSPR, and the ΔT was approximately 32 °C. Although thermal camera analysis is only capable of assessing the bulk temperature of a colloidal dispersion and is unable to reach the nanoscale on the NP surface, this is a reliable indication that the laser source at 532 nm generates a much stronger local heating effect on the

https://doi.org/10.1021/acs.langmuir.3c02994
Langmuir 2024, 40, 5663−5672

surroundings of the AuNPs.[36] This enhancement is attributed mainly to the photothermal heating generated from LSPR-matching excitation. The CALB@AuNPs were stable (non-aggregation or precipitation) after laser irradiation under both conditions, as observed from the UV−vis spectra and TEM images in Figure S2. These findings suggest that photothermal heating resulting in a temperature increase in bulk media up to 30 °C did not destabilize the colloidal dispersion in terms of nonaggregation or precipitation of the NPs and indicate that the ability of the NPs to detach enzymes from the AuNP surface was insufficient, as the colloidal system remains stable. If this was not the case, then we would most likely observe broadening of the LSPR in the UV−vis spectrum and aggregates of AuNPs in the TEM images presented in Figure S2. Furthermore, a previous study[11] showed that free CALB did not respond to light irradiation unless it was in contact with the surface of the AuNPs, which acted as a nanosource of heat[37] for the CALB structure.

However, when we examined the secondary structure of the enzyme by CD spectroscopy, changes in the spectra of the CALB@AuNPs were noted after excitation by green and NIR lasers in comparison to those under nonirradiated conditions (dark), as shown in Figure 2A. Both laser irradiation

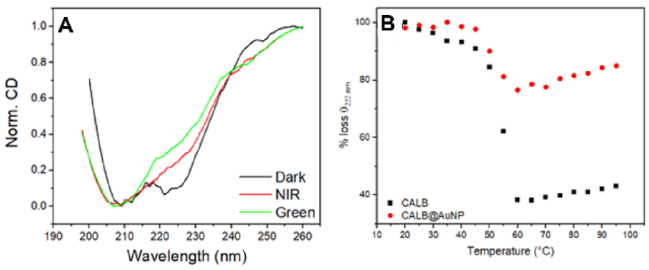

Figure 2. (A) CD spectra of the nanobioconjugate CALB@AuNPs upon nonirradiated conditions (dark) and after exposition to green and NIR lasers, both at a power density of 1.4 W/cm^2 for 20 min. (B) CD signal at λ = 222 nm as a function of temperature (20−95 °C) for free CALB (black dots) and CALB@AuNP (red dots). The temperature was controlled by an external thermal bath attached to the CD spectrophotometer in a closed system.

conditions (λ = 532 and 808 nm) led to modifications in the region around λ = 222 nm compared to the CALB@AuNP sample before any treatment (dark condition). Major modifications were observed after green laser irradiation. The alterations in the CD spectra are mainly related to the changes in the secondary structure of the enzyme, which are usually a result of disturbances induced by the surrounding environment or upon interactions.[38] According to the analysis of the CD data, the percentage of α-helix domains decreased significantly after exposure to NIR (14%) and green (13%) laser irradiation compared to that in the nonirradiated condition (66%). Additionally, the percentages of β-sheet (5%) and random coil (29%) domains under nonirradiated conditions increased under NIR (29% and 57%) and green (31% and 56%) irradiation, respectively (Figure S3). The alterations in the CD spectra suggest that the increase in the temperature in the dispersion medium was a result of the excitation of the AuNPs promoted by either green or NIR lasers, which, in turn, influenced the distortions of the CALB conformation conjugated at the AuNP surface. Indeed, the decrease in the signal at λ = 222 nm typically relies on the loss of secondary structure in terms of the α-helix content present in the overall protein structure.[39] In this way, to correlate the CALB conformation changes with photothermal heating from LSPR excitation of the AuNPs, we analyzed the conformational changes in the nanobioconjugate CALB@AuNPs under increasing temperatures and compared them to the free CALB behavior. Figure 2B shows the CD curves of %loss in ellipticity at 222 nm ($\theta_{222\ nm}$) following a sigmoid pattern carried out from 20 to 95 °C. For CALB@AuNPs, the secondary structure of the enzyme remained stable, with no significant alterations in the signal up to 45 °C. Subsequently, a continuous decrease in the α-helix structure was observed at higher temperatures, particularly from 50 to 60 °C, corresponding to a decrease of almost 25% in the original content. Based on the CD data analyses, the proportions of α-helix, β-sheet, and random coil domains remained stable up to 50 °C, with 61%, 6%, and 33%, respectively. There were slight changes up to 65 °C, with 54% α-helixes, 14% β-sheets, and 32% random coils. However, the proportion of domains underwent a significant change at higher temperatures with a 100% β-sheet structure at 95 °C, which confirmed substantial denaturation from the original enzyme conformation (Figure S4A). In contrast, free CALB showed a more intense loss of α-helix content as the temperature increased, including a prominent decrease in the range of 50−60 °C, for which nearly 60% of the material was lost at 60 °C. Typically, the temperature range of approximately 50−60 °C is related to the denaturation of free CALB, and at higher temperatures, the enzyme structure is distorted until the complete loss of the original conformation occurs, which might explain the continuous change in the 222 nm signal in the CD spectra even at temperatures higher than its denaturation temperature.[40] Indeed, in accordance with the findings from CD data analyses, free CALB presents 99% of its typical α-helix structure at a temperature of 20 °C. However, as the temperature increased, the number of α-helix domains decreased and the number of β-sheet and random coil structures also increased. From the temperature of 60 °C, the conformation of the free CALB was dramatically changed (59% α-helix, 8% β-sheet, and 34% random coil), resulting in the complete loss of its original structure, and likewise for CALB@AuNP at a temperature of 95 °C, the free CALB achieved 100% of β-sheet domains (Figure S4B). Furthermore, our data show that CALB is more thermally stable when adsorbed on the AuNP surface, as was the case for the nanobioconjugates, in agreement with what has been previously reported for different enzymes immobilized onto metallic and nonmetallic nanoparticles.[41]

Interestingly, we observed a reduction in the α-helix content (green line in Figure 2A) soon after exposure to green laser excitation (in resonance with the LSPR of AuNPs), which achieved a temperature of 57 °C (Figure 1C). This temperature is comparable to the temperature range of the enzyme denaturation observed in the CD experiments (50−60 °C; Figure 2B). However, although the highest temperature of green laser irradiation is within the temperature range of CALB denaturation, the impact on the enzyme conformation seems to be different when the enzyme is heated by thermal or photothermal heating. The raw CD spectrum of CALB@AuNPs obtained by thermal heating during the CD temperature ramp assay (Figure S5A) decreased less in intensity as the photothermal temperature increased, as indicated by the signal at λ = 222 nm. This can be a result of a slower rate increase in temperature from thermal heating in comparison to

https://doi.org/10.1021/acs.langmuir.3c02994
Langmuir 2024, 40, 5663−5672

the rapid and instantaneous local increase in the temperature gradient generated from photothermal heating by laser excitation.[42] The local temperature generated from the heating and the dissipation capacity of AuNPs in the surroundings should be a determining factor in the thermal stability of the enzyme conformation located close to the surface.[10] Previous studies that depicted LSPR-driven effects on metallic nanoparticles suggested that there was a significant local increase in the temperature on the surface of the nanoparticle that underwent a photothermal heating process. For instance, in the case of AuNPs, a 61-nanoparticle cluster showed an increase of 95 °C, not considering any convection effects.[43] This LSPR-generated heat decays radially, attenuated by the solvent that surrounds the nanoparticle, and averaging it to a bulk final temperature. Even though this effect leads to an increase in the bulk temperature, the locally generated heat is harsher to the surrounding environment of the NP than the overall increase in the bulk temperature. Thus, according to the results of our CD analyses, we noted important differences in the enzyme conformation when the enzymes were heated by the photothermal effect upon LSPR excitation of AuNPs and when they were heated thermally from an external source. In addition, as the AuNP surface provided a more resilient system to temperature changes than did the free CALB (Figure S5B), we demonstrated that the colloidal stability of the nanobioconjugate was mostly maintained to ensure its conformational properties during laser stimulation.

Thus, we subsequently performed a detailed molecular-level study using Raman spectroscopy to evaluate the modifications in the chemical interactions between the CALB molecule and the AuNP surface that took place under green laser irradiation, which is in resonance with the LSPR excitation. The detailed main modifications to the Raman spectra of CALB and CALB@AuNPs are summarized in Table S1. We began by comparing the Raman spectra of free CALB and CALB@AuNP without laser irradiation to elucidate the major interactions between the components (Figure 3). Our focus

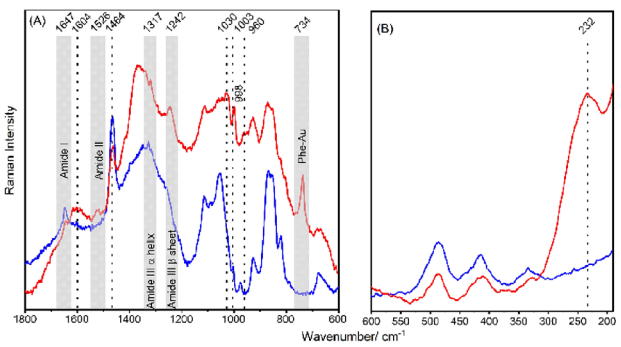

Figure 3. Raman spectra of CALB upon adsorption onto AuNPs. Free CALB (blue) and CALB@AuNP (red) in the wavenumber regions of 1800−600 cm^{-1} (A) and 600−200 cm^{-1} (B).

was on the vibrational bands of amino acids to understand the conformational rearrangements of peptides and proteins.[44,45] Typically, in the 1800−800 cm^{-1} spectral region, the Raman fingerprints correspond to various vibrational bands related to the amide functional groups. These include amide I (∼1650 cm^{-1}), amide II (∼1550 cm^{-1}), and amide III (α-helix at ∼1320 cm^{-1}, and β-sheet at ∼1240 cm^{-1}). Additionally, the vibrational bands observed at 940 and 960 cm^{-1} can also be assigned to the α-helix structure.[46] In the regions at 1647−1642 cm^{-1} and 1360−1318 cm^{-1}, the differences in the signal profiles indicated primary changes of the vibrational modes for both amide I and amide III, respectively. This provided important information into the secondary structure of enzymes,[47] suggesting that the presence of AuNPs induced features of β-sheet structure, as indicated by the signal at 1242 cm^{-1}.[48] This result is closely related to the CD data analysis, which showed that at room temperature (20 °C), free CALB has 0% β-sheet domains (along with 99% α-helices and 1% random coils). However, when CALB is adsorbed on the AuNP surface, forming CALB@AuNP, the proportion increases to up to 6% β-sheet domains (along with 61% α-helices and 33% random coils). There were changes in the vibrational bands, which indicated that AuNPs were adsorbed through interactions with these groups. The shift in Raman band from a sharp signal at 1647 cm^{-1} to a relatively weaker signal at 1642 cm^{-1}, along with broad signals detected at 1629−1512 cm^{-1}, suggests variations in the secondary structure of CALB, which may be associated with molecular reorientation.[49] In the presence of AuNPs, the Raman signals at 1604 and 1526 cm^{-1} are evident in all the spectra. The Raman signal found at 1604 cm^{-1} is usually attributed to the amino acid residues Tyr and Phe,[50] while the signal at 1526 cm^{-1} is associated with the amide II vibrational mode.[51] The amide II mode is related to the vibrational modes ν(CN), δ(NH), and ν(CC), which are tough to detect.[52] Furthermore, the signal at 1465 cm^{-1} attributed to the $\delta(CH_2)$ mode was observed in both spectra.

The amide III vibrational mode is complex to be assigned as the NH band is associated with multiple modes in the region at 1200−1400 cm^{-1}. However, it is important to note that the attribution of vibrational frequencies for secondary structures can be more distinct than that for amides I and II in the spectral range. In this context, the Raman band at 1242 cm^{-1} was attributed to the β-sheet structure with a distinct separation from the amide III mode, which corresponds to the α-helix conformation at 1317 and 960 cm^{-1}.[48] Notably, in the CALB@AuNP spectrum, the strong band at 1030 cm^{-1} can be assigned to the Phe ν_{18a} vibrational mode, which is commonly observed in the Raman spectrum of Phe. Thus, this can indicate that Phe is adsorbed on AuNPs.[53] The Raman band observed at 1003 cm^{-1} in the CALB@AuNP spectrum was found to be shifted to 998 cm^{-1}, indicating a significant interaction between Phe residues and AuNPs. This is because the Raman band at around 1002−1005 cm^{-1} is a characteristic ring mode of phenylalanine.[51] Interestingly, the Raman spectrum of the CALB@AuNPs also exhibited a distinguished band at 734 cm^{-1}, which was not present in the spectrum of free CALB. This notable enhancement in the B_1 symmetry (∼730 cm^{-1}) in the Raman spectrum of CALB@AuNP indicates a direct interaction between the π-electrons of the aromatic Phe ring and the metal surface, confirming that a strong Phe-Au interaction took place in the CALB@AuNP nanobioconjugate.[53] Finally, the signal at 232 cm^{-1} is a typical Raman band for metal-N stretching vibrations, demonstrating that interactions with the N-terminal groups of amino acids can occur. This signal has also been associated with the adsorption of peptides on AuNPs.[54] Hence, based on Raman analyses, it has been revealed that in the CALB@AuNP nanobioconjugate: (i) the AuNPs adsorbed in a manner oriented by N-terminal groups present in the amino acids and because of the Phe-Au interaction and (ii) the secondary

https://doi.org/10.1021/acs.langmuir.3c02994
Langmuir 2024, 40, 5663−5672

structure of CALB undergoes changes upon adsorption/interaction with AuNPs, even prior to any light stimulus.

Subsequently, after a detailed Raman analysis of the CALB@AuNP interactions, we analyzed the effects of green laser irradiation on these interactions (Figure 4). The effect of

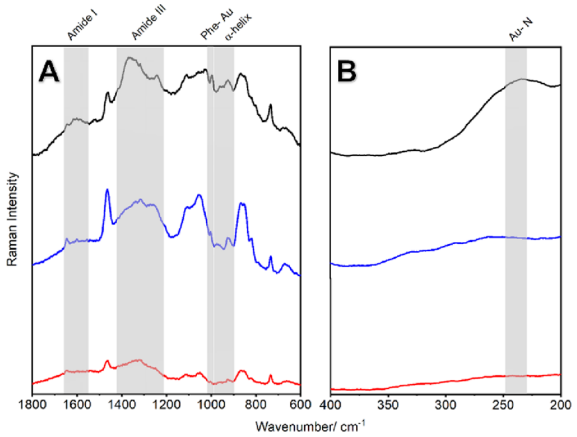

Figure 4. Raman spectra of as-prepared CALB@AuNP (black), after green laser irradiation (λ = 532 nm, 1.4 W/cm^2) for 20 min (blue), and after thermal heating (external temperature) at 55 °C for 20 min (red). Spectra are recorded in the 1800−600 cm^{-1} (A) and 400−200 cm^{-1} (B) regions.

heating at 55 °C for 20 min under nonirradiated conditions was analyzed to determine the effect of temperature on the photothermal heating. It is interesting to note that the Raman intensity decreased considerably across the spectrum after thermal heating (red spectrum). Moreover, the regions attributed to amide I and amide III (regions at approximately 1600 and 1500 cm^{-1}, respectively) responded differently to each of the conditions analyzed. Significative changes in the secondary structure were noticed due to the α-helix structure vibrational attribution, as seen in the Raman bands (region around 924 and 969 cm^{-1}), which is attributed to the vibrations of ν(C−C−N). These differences suggest that compared with those of the as-prepared CALB@AuNPs, the conformational changes and interactions respond differently upon photothermal heating or thermal heating. We made interesting observations when comparing the Raman signals to the CD data. CALB@AuNPs in the dark had a secondary structure composed of 66% α-helix, 5% β-sheet, and 29% random coil domains. However, when we heated the sample to 55 °C by external thermal heating, we observed proportions of 55% α-helixes, 11% β-sheets, and 34% random coils. After exposure to green laser irradiation, we observed a more drastic alteration, detecting 13% α-helix, 31% β-sheet, and 56% random coil domains. These results indicated that green laser irradiation generated more significant distortions in the CALB structure at the nanobioconjugate CALB@AuNP than at a similar temperature using external thermal heating. Furthermore, these results indicate that either LSPR effects may contribute via other mechanisms beyond temperature effects or that the local temperature produced by photothermal heating through LSPR excitation at the AuNP surface can uniquely promote conformational changes in the CALB. Therefore, from the Raman data, we can confirm the important alterations in the amide I and amide III (α-helix and β-sheet, respectively) modes due to the CALB adsorption on AuNPs and subsequent photothermal treatments. The temperature ramp analysis of the CD indicated that the 60% α-helix domains in the CALB@AuNPs remained unchanged up to 50 °C. This suggests that the CALB structure's α-helix domains may be better preserved when adsorbed onto AuNPs, even upon environmental changes.

To gain further insight into the effect of the temperature increase driven by the LSPR stimulus, we conducted molecular dynamics (MD) simulations to determine the unfolding of free CALB and CALB@AuNPs via CD and Raman analyses. Free CALB (PDB: 1TCA) in solution at different arbitrary temperatures (T*, in LJ units) was analyzed through coarse-grained molecular dynamics simulations using a large-scale atomic/molecular massively parallel simulator (LAMMPS) following a previously developed procedure to account for the electric and H-bond interactions between the NPs and the adsorbing protein.[29,55] To evaluate the enzymatic conformational changes in both the free and AuNP-adsorbed conditions at different temperatures, we followed the evolution of the root-mean-square displacement (RMSD) and the radial distribution function of the overall structure of the enzyme. Additionally, during the time course, the catalytic triad of CALB, which is composed of the residues Ser105-Asp187-His224, was monitored to determine the conformation at which the activity decreases as a function of the enzyme denaturation.

Figure 5A and Figure 5B show the time evolutions of free CALB and CALB@AuNP, respectively. The CALB structure remained mostly unchanged at temperatures below T* = 4, regardless of whether it was free or interacting with the AuNPs. However, temperatures above T* = 5 caused significant shifts

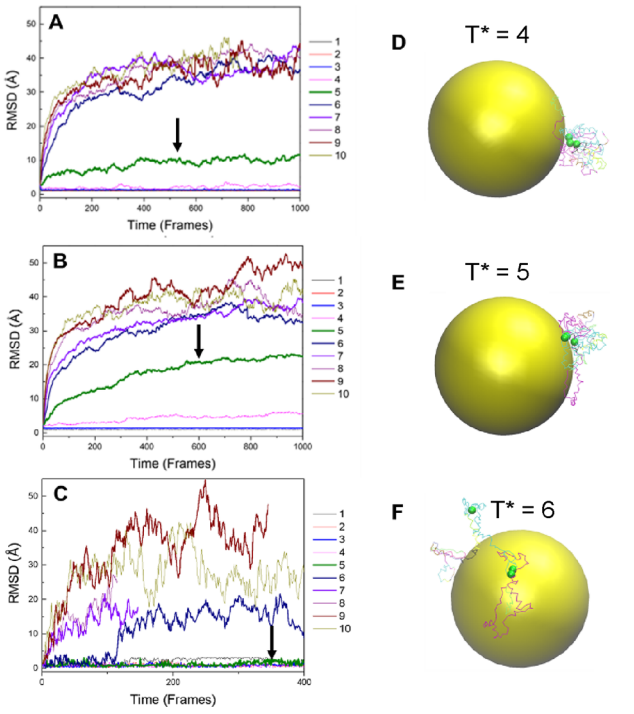

Figure 5. (Top) RMSD of free CALB (A) and CALB@AuNP (B) upon different arbitrary temperatures (ranging from 1 to 10 in LJ units). In panel (C), the RMSD of the catalytic triad is only upon absorption at different temperatures. (Left) The black arrows in the figures point out the curve corresponding to the RMSD at T = 5. (Right) Snapshots of the enzyme absorbed onto the surface (in green, the catalytic triad) at (D) T* = 4, (E) T* = 5, and (F) T* = 6.

https://doi.org/10.1021/acs.langmuir.3c02994
Langmuir 2024, 40, 5663−5672

in RMSD, which indicates that the CALB structure denatured independently of the presence of AuNPs. At this temperature, CALB@AuNPs experienced a greater displacement in RMSD than free CALB. The fluctuations in the RMSD at $T^* = 4$ were small, but they suggest that the enzyme is close to the unfolding temperature. This reproduces the folded−unfolded transition at lower temperatures than when adsorbed on the AuNPs, as also observed experimentally for CALB@AuNPs with CD (Figure 2B). In this context, the results obtained from the MD simulations showed a similar tendency to be observed for experimental temperatures <50 °C and >50 °C.

The data presented in Figure S6 reinforced the tendency of denaturation that was observed earlier. This is in agreement with the coarse-grained simulation and the CD temperature curve at 222 nm (Figure 2B).[40] It should be noted that both CD signal decreases observed experimentally coincided with the numerical results for structural changes estimated via the RMSD as the temperature increased. Although these data sets can only be associated indirectly, both data from the CD temperature curve and RMSD tendencies showed a sigmoidal-type curve profile as a function of temperature increase. This is indicative that the CALB structure is stable at low temperatures and desaturates at higher temperatures. It is important to notice that 10 different numerical experiments were performed with different initial dispositions of the enzyme to calculate an average final RMSD. The standard deviations supported that our estimations for single numerical experiment runs were satisfactory. The comparison also showed that the simulation temperature scale was consistent with the experimental temperature scale. In particular, we determined that the unfolding temperature in the simulation was $T^* = 5$, corresponding to an experimental temperature of $T = 55$ °C. Again, this indirect comparison is intended to show that there is a correlation between the observed deformation of the overall structure of the enzyme and the CD signal in both the presence and absence of the NP.

Figure 5C illustrates the catalytic triad Ser105-Asp187-His224 present in the CALB structure on the surface of AuNPs, represented at different arbitrary temperatures. This representation shows that while the enzyme is completely unfolded for $T^* > 5$, the triad indicates high stability and proximity to the NP. Interestingly, the catalytic moiety of CALB remained close to the NP when at low temperatures, as evidenced by the close-to-zero RMSD for $T^* < 6$ in Figure S7.[56] However, the RMSD showed greater displacement at $T^* = 6$ and above, which can be indicative of conformational loss with separation among the residues developed over time. This result may suggest that the stability of the triad subdomain is greater than the rest of the enzyme's structure. In Figure S8, the distances between the triad residues were noticed for free CALB and CALB@AuNPs. At higher temperatures, a broader distribution of radial distances was observed, until the temperature where the denaturation occurred and the residues were too far apart was reached to evaluate the distance.

A change in the conformation of the enzyme following a temperature increase can be understood as a slight variation in the RMSD, which results in a greater exposure of the catalytic triad to the media. The data reported here can be explained through three main facts occurring simultaneously: (i) CALB is stable either in the presence or absence of NPs at temperatures below 50 °C, (ii) the catalytic triad remains stable, and (iii) the catalytic triad continued close to the surface of AuNPs, within the same temperature range. It is worth noting that our simulation did not account for temperature gradients that irradiation might create. In summary, MD data indicate that the catalytic triad Ser105-Asp187-His224 is stable and exposed upon local heat and on adsorbed on the AuNPs.

CONCLUSIONS

In conclusion, the colloidal stability and molecular physicochemical interactions upon adsorption, thermal, and photothermal heating promoted by LSPR excitation under green (in resonance) and NIR (out of resonance) laser stimuli between a model enzyme (CALB) and AuNPs were determined by converging analyses of CD, Raman, and MD simulations. Important differences were found in the enzyme secondary structure in terms of α-helix content and denaturation of the structure because of either the adsorption of CALB onto AuNPs or the thermal heat source. Even though the system was exposed to a similar temperature, the instantaneous increase in the local temperature gradient generated from photothermal heating by in-resonance laser irradiation played a significant role in the original secondary structure of CALB rather than thermal heating. These data indicate that LSPR excitation at the AuNP surface can uniquely promote conformational changes in the CALB and may even contribute through other plasmonic mechanisms beyond the temperature enhancement. Raman analysis revealed that the signals for the amide I and III (α-helix and β-sheet) modes were significantly induced upon CALB adsorption on AuNPs and subsequent photothermal treatment. MD calculations suggested the consequent exposure of the highly stable catalytic triad Ser105-Asp187-His224 to the heat generated by LSPR. Since the simulations accounted for temperature effects only, further work is needed to address the impact of CALB conformational changes resulting from the rapid increase in temperature on the kinetics of CALB@AuNP enzyme-catalyzed reactions upon green laser excitation. However, our results suggest that the dynamic effect of the CALB structure is governed mainly by photothermal heating rather than thermal heating. The findings highlighted from this study introduce fundamental concepts about the effect of laser stimuli on interactions at the nano−bio interface, which provides important information for the advancement of studies using the potential of LSPR to remotely control enzyme properties. We envision that these findings will be highly valuable for plasmonic biocatalysis studies and other remote-controlled systems for manipulating protein properties for improved performance and biomedical applications.

ASSOCIATED CONTENT

Supporting Information

The Supporting Information is available free of charge at https://pubs.acs.org/doi/10.1021/acs.langmuir.3c02994.

Additional information on the characterization of the synthesized AuNPs, laser effect on CALB@AuNPs, secondary structure content analyses of CALB@AuNPs, CD spectra obtained from the temperature ramp assay, RMSD details, MD analysis details, and table with Raman assignments (PDF)

https://doi.org/10.1021/acs.langmuir.3c02994
Langmuir 2024, 40, 5663−5672

AUTHOR INFORMATION

Corresponding Authors

Heloise Ribeiro de Barros − *Department of Fundamental Chemistry, Institute of Chemistry, University of São Paulo, São Paulo 05508-000, São Paulo, Brasil; CIC biomaGUNE and CIBER-BBN, Donostia-San Sebastián 2014, Spain;* orcid.org/0000-0003-2700-7803; Email: barroshr@usp.br

Susana I. Cordoba de Torresi − *Department of Fundamental Chemistry, Institute of Chemistry, University of São Paulo, São Paulo 05508-000, São Paulo, Brasil;* orcid.org/0000-0003-3290-172X; Email: storresi@iq.usp.br

Authors

Rafael Trivella Pacheco da Silva − *Department of Fundamental Chemistry, Institute of Chemistry, University of São Paulo, São Paulo 05508-000, São Paulo, Brasil;* orcid.org/0000-0002-1762-793X

Rafaella Fernandes − *Department of Fundamental Chemistry, Institute of Chemistry, University of São Paulo, São Paulo 05508-000, São Paulo, Brasil*

Jhoan Toro-Mendoza − *CIC biomaGUNE and CIBER-BBN, Donostia-San Sebastián 2014, Spain; Centro de Biomedicina Molecular, Instituto Venezolano de Investigaciones Científicas, Caracas 1020, Venezuela;* orcid.org/0000-0003-4916-7445

Ivan Coluzza − *Center for Theoretical Biological Physics, Rice University, Houston, Texas 77005, United States*

Marcia L. A. Temperini − *Department of Fundamental Chemistry, Institute of Chemistry, University of São Paulo, São Paulo 05508-000, São Paulo, Brasil;* orcid.org/0000-0003-4655-6891

Complete contact information is available at: https://pubs.acs.org/10.1021/acs.langmuir.3c02994

Author Contributions

H.R.d.B. conceived and administered the project, acquired the TEM micrographs, conducted the CD assays, and wrote the original draft. R.T.P.d.S. was responsible for the data curation and project administration. Both R.T.P.d.S. and H.R.d.B. led the execution of this study. R.F. acquired the Raman data, and M.L.A.T. analyzed the Raman results. J.T.-M. and I.C. acquired the MD data and analyzed the results. S.I.C.d.T. supervised the project.

Notes

The authors declare no competing financial interest.

ACKNOWLEDGMENTS

The authors thank the Brazilian agency CNPq (#302173/2016-1) and the São Paulo Research Foundation FAPESP (2021/00675-4, 2016/21070-5, and 2018/13492-2) for financial support. H.R.d.B. acknowledges FAPESP for the fellowships granted (2019/09668-0 and 2017/20892-4). R.T.P.d.S. also thanks CAPES for the fellowship (88882.328241/2019-01). R.F. thanks FAPESP for the fellowship (2018/25422-9). We are thankful for the support of the computing infrastructure of the i2BASQUE academic network and the ATLAS machine at the DIPC. This research was supported by the Spanish Ministerio de Economía y Competitividad (MINECO) (FIS2017-89471-R to I.C.). This research was supported by the Programa Red Guipuzcoana de Ciencia, Tecnología e Información (2019-CIEN-000051-01 to I.C.). We thank Prof. Luis M. Liz-Marzán for kindly providing access to the facilities at CIC biomaGUNE. Funding is acknowledged by the Spanish State Research Agency (Project MDM-2017-0720).

ABBREVIATIONS

NP, nanoparticle; AuNP, gold nanoparticle; CALB, *Candida antarctica* fraction B; LSPR, localized surface plasmon resonance; CD, circular dichroism; MD, molecular dynamics; LAMMPS, atomic/molecular massively parallel simulator; RMSD, root-mean-square displacement; NIR, near-infrared; TEM, transmission electron microscopy

REFERENCES

(1) Bhaumik, A.; Shearin, A. M.; Delong, R.; Wanekaya, A.; Ghosh, K. Probing the Interaction at the Nano-Bio Interface Using Raman Spectroscopy: ZnO Nanoparticles and Adenosine Triphosphate Biomolecules. *J. Phys. Chem. C* **2014**, *118* (32), 18631−18639.

(2) Nel, A. E.; Madler, L.; Velegol, D.; Xia, T.; Hoek, E. M. V.; Somasundaran, P.; Klaessig, F.; Castranova, V.; Thompson, M. Understanding biophysicochemical interactions at the nano-bio interface. *Nat. Mater.* **2009**, *8* (7), 543−557.

(3) Mahmoudi, M.; Abdelmonem, A. M.; Behzadi, S.; Clement, J. H.; Dutz, S.; Ejtehadi, M. R.; Hartmann, R.; Kantner, K.; Linne, U.; Maffre, P.; et al. Temperature: The "Ignored" Factor at the NanoBio Interface. *ACS Nano* **2013**, *7* (8), 6555−6562.

(4) Cai, P. Q.; Zhang, X. Q.; Wang, M.; Wu, Y. L.; Chen, X. D. Combinatorial Nano-Bio Interfaces. *ACS Nano* **2018**, *12* (6), 5078−5084.

(5) da Silva, R. T. P.; Ribeiro de Barros, H.; Sandrini, D. M. F.; Córdoba de Torresi, S. I. Stimuli-Responsive Regulation of Biocatalysis through Metallic Nanoparticle Interaction. *Bioconjugate Chem.* **2022**, *33* (1), 53−66.

(6) Wasserberg, D.; Cabanas-Danes, J.; Prangsma, J.; O'Mahony, S.; Cazade, P. A.; Tromp, E.; Blum, C.; Thompson, D.; Huskens, J.; Subramaniam, V.; et al. Controlling Protein Surface Orientation by Strategic Placement of Oligo-Histidine Tags. *ACS Nano* **2017**, *11* (9), 9068−9083.

(7) Bolaños, K.; Celis, F.; Garrido, C.; Campos, M.; Guzmán, F.; Kogan, M. J.; Araya, E. Adsorption of bovine serum albumin on gold nanoprisms: interaction and effect of NIR irradiation on protein corona. *J. Mater. Chem. B* **2020**, *8* (37), 8644−8657.

(8) Koshkina, O.; Lang, T.; Thiermann, R.; Docter, D.; Stauber, R. H.; Secker, C.; Schlaad, H.; Weidner, S.; Mohr, B.; Maskos, M.; et al. Temperature-Triggered Protein Adsorption on Polymer-Coated Nanoparticles in Serum. *Langmuir* **2015**, *31* (32), 8873−8881.

(9) An, J.; Li, G. L.; Zhang, Y. F.; Zhang, T. B.; Liu, X. L.; Gao, F.; Peng, M. L.; He, Y.; Fan, H. M. Recent Advances in Enzyme-Nanostructure Biocatalysts with Enhanced Activity. *Catalysts* **2020**, *10* (3), 338.

(10) de Barros, H. R.; López-Gallego, F.; Liz-Marzán, L. M. Light-Driven Catalytic Regulation of Enzymes at the Interface with Plasmonic Nanomaterials. *Biochemistry* **2020**, *60* (13), 991−998.

(11) de Barros, H. R.; García, I.; Kuttner, C.; Zeballos, N.; Camargo, P. H. C.; de Torresi, S. I. C.; López-Gallego, F.; Liz-Marzán, L. M. Mechanistic insights on the light-driven catalysis of an immobilized lipase on plasmonic nanomaterials. *ACS Catal.* **2020**, *11*, 414−423.

(12) Blankschien, M. D.; Pretzer, L. A.; Huschka, R.; Halas, N. J.; Gonzalez, R.; Wong, M. S. Light-Triggered Biocatalysis Using Thermophilic Enzyme-Gold Nanoparticle Complexes. *ACS Nano* **2013**, *7* (1), 654−663.

(13) Guo, S. J.; Li, H.; Liu, J.; Yang, Y. M.; Kong, W. Q.; Qiao, S.; Huang, H.; Liu, Y.; Kang, Z. H. Visible-Light-Induced Effects of Au Nanoparticle on Laccase Catalytic Activity. *ACS Appl. Mater. Interfaces* **2015**, *7* (37), 20937−20944.

(14) Tadepalli, S.; Yim, J.; Madireddi, K.; Luan, J.; Naik, R. R.; Singamaneni, S. Gold Nanorod-Mediated Photothermal Enhance-

ment of the Biocatalytic Activity of a Polymer-Encapsulated Enzyme. *Chem. Mater.* **2017**, *29* (15), 6308−6314.
(15) Li, W.; Liu, D. N.; Geng, X.; Li, Z. Q.; Gao, R. J. Real-time regulation of catalysis by remote-controlled enzyme-conjugated gold nanorod composites for aldol reaction-based applications. *Catal. Sci. Technol.* **2019**, *9* (9), 2221−2230.
(16) da Silva, R. T. P.; de Barros, H. R.; Fernandes, R. F.; Temperini, M. L. A.; Cordoba de Torresi, S. I. Cytochrome C with Peroxidase-like Activity Supported on Plasmonic AuNPs: Improved Stability and Enhanced Nanobioplasmonic Catalytic Conversion. *ChemCatChem.* **2023**, *15* (4), 1−8.
(17) Carone, A.; Emilsson, S.; Mariani, P.; Desert, A.; Parola, S. Gold nanoparticle shape dependence of colloidal stability domains. *Nanoscale Adv.* **2023**, *5* (7), 2017−2026.
(18) Baffou, G.; Quidant, R. Nanoplasmonics for chemistry. *Chem. Soc. Ver.* **2014**, *43* (11), 3898−3907.
(19) Silva, R. T. P. D. Nanobiocatalysts: Nanozymes and Nanobioconjugates in Heterogeneous Catalysis and Electrocatalysis. PhD thesis, University of São Paulo, 2022. DOI: 10.11606/T.46.2022.tde-02122022−165753. https://www.teses.usp.br/teses/disponiveis/46/46136/tde-02122022-165753/pt-br.php (accessed 15/02/2024).
(20) Bradford, M. M. Rapid and Sensitive Method for Quantitation of Microgram Quantities of Protein Utilizing Principle of Protein-Dye Binding. *Anal. Biochem.* **1976**, *72* (1−2), 248−254.
(21) Turkevich, J.; Stevenson, P. C.; Hillier, J. A Study of the Nucleation and Growth Processes in the Synthesis of Colloidal Gold. *Discuss. Faraday Soc.* **1951**, *11*, 55−75.
(22) Hendel, T.; Wuithschick, M.; Kettemann, F.; Birnbaum, A.; Rademann, K.; Polte, J. In Situ Determination of Colloidal Gold Concentrations with UV-Vis Spectroscopy: Limitations and Perspectives. *Anal. Chem.* **2014**, *86* (22), 11115−11124.
(23) Whitmore, L.; Wallace, B. A. DICHROWEB, An Online Server for Protein Secondary Structure Analyses From Circular Dichroism Spectroscopic Data. *Nucleic Acids Res.* **2004**, *32*, W668−W673.
(24) Plimpton, S. Fast Parallel Algorithms For Short-Range Molecular-Dynamics. *J. Computat. Phys.* **1995**, *117* (1), 1−19.
(25) *LAMMPS*. https://www.lammps.org/#gsc.tab=0 (accessed 01/12/2023).
(26) Baumketner, A.; Jewett, A.; Shea, J. E. Effects of confinement in chaperonin assisted protein folding: Rate enhancement by decreasing the roughness of the folding energy landscape. *J. Mol. Biol.* **2003**, *332* (3), 701−713.
(27) Onuchic, J. N.; Wolynes, P. G. Theory of protein folding. *Curr. Opin. Struct. Biol.* **2004**, *14* (1), 70−75.
(28) Ohshima, H.; Healy, T. W.; White, L. R. Accurate Analytic Expressions for the Surface-Charge Density Surface-Potential Relationship and Double-Layer Potential Distribution for a Spherical Colloidal Particle. *J. Colloid Interface Sci.* **1982**, *90* (1), 17−26.
(29) Toro-Mendoza, J.; Maio, L.; Gallego, M.; Otto, F.; Schulz, F.; Parak, W. J.; Sanchez-Cano, C.; Coluzza, I. Bioinspired Polyethylene Glycol Coatings for Reduced Nanoparticle-Protein Interactions. *ACS Nano* **2023**, *17* (2), 955−965.
(30) de Barros, H.; Santos, M.; Barbosa, L.; Piovan, L.; Riegel-Vidotti, I. Physicochemical Study of the Interaction between Gold Nanoparticles and Lipase from Candida sp. (CALB): Insights into the Nano-Bio Interface. *J. Braz. Chem. Soc.* **2019**, *30* (10), 2231−2242.
(31) Baumann, V.; Habeeb Muhammed, M. A.; Blanch, A. J.; Dey, P.; Rodríguez-Fernández, J. Biomolecules in Metal and Semiconductor Nanoparticle Growth. *Isr. J. Chem.* **2016**, *56* (4), 195−213.
(32) Irani, M.; Tornvall, U.; Genheden, S.; Larsen, M. W.; Hatti-Kaul, R.; Ryde, U. Amino Acid Oxidation of Candida antarctica Lipase B Studied by Molecular Dynamics Simulations and Site-Directed Mutagenesis. *Biochemistry* **2013**, *52* (7), 1280−1289.
(33) Sasaki, Y. C.; Yasuda, K.; Suzuki, Y.; Ishibashi, T.; Satoh, I.; Fujiki, Y.; Ishiwata, S. Two-dimensional arrangement of a functional protein by cysteine-gold interaction: Enzyme activity and characterization of a protein monolayer on a gold substrate. *Biophys. J.* **1997**, *72* (4), 1842−1848.
(34) Mendes, G. R.; Modenez, I. D.; Cagnani, G. R.; Colombo, R. N. P.; Crespilho, F. N. Exploring Enzymatic Conformational Dynamics at Surfaces through μ-FTIR Spectromicroscopy. *Anal. Chem.* **2023**, *95* (30), 11254−11262.
(35) Yu, J.; Becker, M. L.; Carri, G. A. The Influence of Amino Acid Sequence and Functionality on the Binding Process of Peptides onto Gold Surfaces. *Langmuir* **2012**, *28* (2), 1408−1417.
(36) Lv, S. J.; Du, Y. P.; Wu, F. T.; Cai, Y. C.; Zhou, T. Review on LSPR assisted photocatalysis: effects of physical fields and opportunities in multifield decoupling. *Nanoscale Adv.* **2022**, *4* (12), 2608−2631.
(37) Baffou, G.; Quidant, R. Thermo-plasmonics: using metallic nanostructures as nano-sources of heat. *Laser Photonics Rev.* **2013**, *7* (2), 171−187.
(38) Yoneda, J. S.; Cardoso, M. B. Nanoparticle-induced conformational changes in protein corona revealed by circular dichroism spectroscopy. *Nanomedicine* **2023**, *18* (9), 709−711.
(39) Kelly, S. M.; Jess, T. J.; Price, N. C. How to study proteins by circular dichroism. *Biochim. Biophys. Acta, Proteins Proteomics* **2005**, *1751* (2), 119−139.
(40) Rabbani, G.; Ahmad, E.; Khan, M. V.; Ashraf, M. T.; Bhat, R.; Khan, R. H. Impact of structural stability of cold adapted Candida antarctica lipase B (CaLB): in relation to pH, chemical and thermal denaturation. *RSC Adv.* **2015**, *5* (26), 20115−20131.
(41) Arsalan, A.; Younus, H. Enzymes and nanoparticles: Modulation of enzymatic activity via nanoparticles. *International J. Biol. Macromol.* **2018**, *118*, 1833−1847.
(42) Kang, P.; Chen, Z.; Nielsen, S. O.; Hoyt, K.; D'Arcy, S.; Gassensmith, J. J.; Qin, Z. Molecular Hyperthermia: Spatiotemporal Protein Unfolding and Inactivation by Nanosecond Plasmonic Heating. *Small* **2017**, *13* (36), 1−7.
(43) Borah, R.; Verbruggen, S. W. Coupled Plasmon Modes in 2D Gold Nanoparticle Clusters and Their Effect on Local Temperature Control. *J. Phys. Chem. C* **2019**, *123* (50), 30594−30603.
(44) Kong, J.; Yu, S. Fourier transform infrared spectroscopic analysis of protein secondary structures. *Acta Biochim. Biophys. Sin.* **2007**, *39* (8), 549−559.
(45) Tuma, R. Raman spectroscopy of proteins: from peptides to large assemblies. *J. Raman Spectrosc.* **2005**, *36* (4), 307−319.
(46) Blanpain-Avet, P.; Hedoux, A.; Guinet, Y.; Paccou, L.; Petit, J.; Six, T.; Delaplace, G. Analysis by Raman spectroscopy of the conformational structure of whey proteins constituting fouling deposits during the processing in a heat exchanger. *J. Food Eng.* **2012**, *110* (1), 86−94.
(47) Hernandez, B.; Lopez-Tobar, E.; Sanchez-Cortes, S.; Coic, Y. M.; Baron, B.; Chenal, A.; Kruglik, S. G.; Pfluger, F.; Cohen, R.; Ghomi, M. From bulk to plasmonic nanoparticle surfaces: the behavior of two potent therapeutic peptides, octreotide and pasireotide. *Phys. Chem. Chem. Phys.* **2016**, *18* (35), 24437−24450.
(48) Seo, J. A.; Hedoux, A.; Guinet, Y.; Paccou, L.; Affouard, F.; Lerbret, A.; Descamps, M. Thermal Denaturation of Beta-Lactoglobulin and Stabilization Mechanism by Trehalose Analyzed from Raman Spectroscopy Investigations. *J. Phys. Chem. B* **2010**, *114* (19), 6675−6684.
(49) Carcamo, J. J.; Aliaga, A. E.; Clavijo, R. E.; Branes, M. R.; Campos-Vallette, M. M. Raman study of the shockwave effect on collagens. *Spectrochim. Acta, Part A* **2012**, *86*, 360−365.
(50) Rothschild, K. J.; Andrew, J. R.; Degrip, W. J.; Stanley, H. E. Opsin Structure Probed by Raman-Spectroscopy of Photoreceptor Membranes. *Science* **1976**, *191* (4232), 1176−1178.
(51) Rygula, A.; Majzner, K.; Marzec, K. M.; Kaczor, A.; Pilarczyk, M.; Baranska, M. Raman Spectroscopy of Proteins: A Review. *J. Raman Spectrosc.* **2013**, *44* (8), 1061−1076.
(52) Ortiz, C.; Zhang, D. M.; Ribbe, A. E.; Xie, Y.; Ben-Amotz, D. Analysis of insulin amyloid fibrils by Raman spectroscopy. *Biophys. Chem.* **2007**, *128* (2−3), 150−155.
(53) Podstawka, E.; Ozaki, Y.; Proniewicz, L. M. Part III: Surface-enhanced Raman scattering of amino acids and their homodipeptide

monolayers deposited onto colloidal gold surface. *Appl. Spectrosc.* **2005**, *59* (12), 1516−1526.
(54) Lopez-Tobar, E.; Hernandez, B.; Gomez, J.; Chenal, A.; Garcia-Ramos, J. V.; Ghomi, M.; Sanchez-Cortes, S. Anchoring Sites of Fibrillogenic Peptide Hormone Somatostatin-14 on Plasmonic Nanoparticles. *J. Phys. Chem. C* **2015**, *119* (15), 8273−8279.
(55) Meesaragandla, B.; Garcia, I.; Biedenweg, D.; Toro-Mendoza, J.; Coluzza, I.; Liz-Marzan, L. M.; Delcea, M. H-Bonding-mediated binding and charge reorganization of proteins on gold nanoparticles. *Phys. Chem. Chem. Phys.* **2020**, *22* (8), 4490−4500.
(56) Cen, Y.; Singh, W.; Arkin, M.; Moody, T. S.; Huang, M.; Zhou, J.; Wu, Q.; Reetz, M. T. Artificial cysteine-lipases with high activity and altered catalytic mechanism created by laboratory evolution. *Nat. Commun.* **2019**, *10*, 3198.

https://doi.org/10.1021/acs.langmuir.3c02994
Langmuir 2024, 40, 5663−5672